Check for updates

View Article Online
View Journal

NJC

New Journal of Chemistry

A journal for new directions in chemistry

Accepted Manuscript

This article can be cited before page numbers have been issued, to do this please use: M. Banerjee, M. Ghosh, S. Ta, S. Ghosh and D. Das, *New J. Chem.*, 2020, DOI: 10.1039/D0NJ03024D.

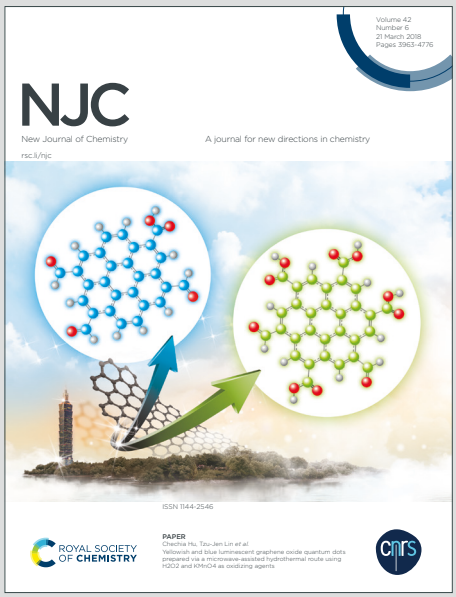

This is an Accepted Manuscript, which has been through the Royal Society of Chemistry peer review process and has been accepted for publication.

Accepted Manuscripts are published online shortly after acceptance, before technical editing, formatting and proof reading. Using this free service, authors can make their results available to the community, in citable form, before we publish the edited article. We will replace this Accepted Manuscript with the edited and formatted Advance Article as soon as it is available.

You can find more information about Accepted Manuscripts in the Information for Authors.

Please note that technical editing may introduce minor changes to the text and/or graphics, which may alter content. The journal's standard Terms & Conditions and the Ethical guidelines still apply. In no event shall the Royal Society of Chemistry be held responsible for any errors or omissions in this Accepted Manuscript or any consequences arising from the use of any information it contains.

Please do not adjust margins

Journal Name

ROYAL SOCIETY OF CHEMISTRY View Article Online
DOI: 10.1039/D0NJ03024D

ARTICLE

Tuning of uracil derivative for AIE based detection of pyrene at nano-molar level: Single crystal X-ray structure and DFT support

Mahuya Banerjee[a], Milan Ghosh,[a] Sabyasachi Ta,[a] Subhasis Ghosh[a] and Debasis Das*[a]

Also 4Received 00th January 20xx,
Accepted 00th January 20xx

DOI: 10.1039/x0xx00000x

www.rsc.org/

Single crystal X-ray structurally characterized azo-uracil derivative (L) is explored for selective detection of pyrene *via* aggregation induced emission (AIE) with 99-fold fluorescence enhancement. In presence of pyrene, non-fluorescent L emits green light that allows to detect as low as 3.6×10^{-9} M pyrene. Three model probes (L1, L2 and L3) have been employed to support the proposed sensing mechanism. The silica immobilized L efficiently removes pyrene from its reservoir.

KEYWORDS: Azo-uracil, sensor, nano-molar, fluorescence, naked eye, AIE, pyrene.

1. Introduction

Development of optical probe for selective detection and estimation of toxic small molecules is an emerging research area.[1-2] Economic evolution and energy exploitation demands consumption of significant amount of polyaromatic hydrocarbons (PAHs) that lead to environment contamination.[3] This is due to incomplete combustion of PAHs,[4-5] most of which are carcinogenic/ mutagenic.[6-8a] Extreme harmful effects like cell damaging, cyto-toxicity, mutagenicity, and nerve damaging effects have brought them under the umbrella, "ten most toxic classes" of organic compounds by U.S. Centre for Disease Control and Prevetion.[8b] They are capable to change the protein and nucleic acid structures.[9-10] Pyrene, one of the most important members of PAHs family, imparts toxicity in living organism.[11-12] Its epoxides are extremely toxic, mutagenic and/or carcinogenic to microorganisms and higher systems including human.[13] The exposure to pyrene generates nephropathy, kidney damage, and haematological changes.[14-15] Several pyrene derivatives cause skin, lung, bladder, liver and stomach cancer.[16-18] The hydrophobic pyrene accumulates in cell membrane and lipid tissues.[19] The soil contaminated with pyrene is alarming for food security, particularly for grains, fruits, vegetables, drinking water and meat.[20-22] The benzo-pyrene (BaP) binds to DNA to cause lung cancer, damage white blood cell, reproductive system and CYP450 enzymes.[23-27] Dry cleaning of garments may lead to pyrene toxicity.[28-30] Its unique spectral feature, particularly high extinction coefficient is useful to gather information about molecular organization and protein conformation.[31-34] The pyrene derivatives have been used as fluorescence probe to study the solvent micro-environment.[35] Hence, trace level

Department of Chemistry, The University of Burdwan, Burdwan, 713104, West Bengal, India.
Correspondence: <ddas100in@yahoo.com2>; phone, +91-342- 2533913; fax, +91-342-2530452

Published on 12 August 2020. Downloaded by Cornell University Library on 8/15/2020 11:04:24 AM.

New Journal of Chemistry Accepted Manuscript

Please do not adjust margins

View Article Online
DOI: 10.1039/D0NJ03024D

Published on 12 August 2020. Downloaded by Cornell University Library on 8/15/2020 11:04:24 AM.

selective detection and estimation of pyrene is demanding. However, similarities of pyrene with other PAHs is the primary obstacle for its selective detection. For example, pyrene and most of the PAHs are prone to aggregation that causes shift of the emission peak that hinders their selective recognition.[36-37] Pyrene is primarily determined by chromatography, particularly high-performance liquid chromatography.[38-39] However, fluorescence technique is much more superior to other methods in terms of sample preparation, operational simplicity, inexpensive methodology, rapidity, direct visualization/perception and higher sensitivity.[40-42]

Recently, graphene quantum dot is employed for fluorescence recognition of pyrene in aqueous medium[51b]. Moreover, a pyrene–antipyrine conjugate has been used for detection of pyrene in DMSO/H_2O (4/1) media.[43]

On the other hand, uracil derivatives are primary target for several organic synthesis[44] and used as drug carrier.[45-52a] Its unique, non-toxic properties inspired to study photo-physical interactions with living organism. Azo compounds play significant role in several biological reactions, like protein synthesis, inhibition of carcinogenesis and nitrogen fixation.[51b] Interestingly, number of hetero atoms, ring size and substituent significantly influence over the π-acidity of azoheterocycle that regulate its physical, chemical, electrochemical and photo-physical properties.[51c] It is noteworthy to mention that we have reported Cu(II) catalyzed cyclization of azouracil to anticancer active triazole derivative very recently.[51d]

Herein, we report another azouracil derivative (L) for detection of nano-molar pyrene *via* aggregation induced emission. Moreover, three model probes, *viz.* L1, L2 and L3 have been designed, synthesised and employed to unveil the plausible mechanism of interaction. Interestingly, silica immobilized probe (L) efficiently removes pyrene from real samples.

2. Results and discussion

Four new compounds (L, L1, L2 and L3) have been synthesised (yield, 93-96%) and characterized by different spectroscopic techniques (Scheme1, Figure S1-S17, ESI). Among them, L shows very weak emission at 373 nm upon excitation at 336 nm (Figure S5, ESI). On the other hand, L1, L2 and L3 exhibit weak emission at 396 nm, 388 nm and 351 nm upon excitation at 302 nm, 300 nm and 282 nm respectively (Figure S9, S13 and S17, ESI).

The absorption spectrum of L (20 μM, DMSO/H_2O, 4/1, v/v, HEPES buffer, pH 7.4) exhibits peaks at 256 nm (ε, 8.8×10^5 M^{-1} cm^{-1}) and 403 nm (ε, 5.66×10^3 M^{-1} cm^{-1}), assigned to π–π* and n–π* transitions respectively.[52]

2.1. Single crystal X-ray structure of L

The ORTEP view of L along with atom numbering scheme is presented in Figure 1. The refinement parameters of L that crystallizes in 'P-1' space group (CCDC No. 1869304) are presented in Table S1-S2 (ESI). The azo bond (N3–N001) distance, ~1.315Å is comparable to literature value (1.28–1.30Å).[45] It is to be noted that in L, one N is protonated (N7) while Cl^- presents as counter ion which is primarily responsible for hydrogen bonding. The packing diagram with intermolecular hydrogen bonding is shown in Figure S18, ESI. Other crystal parameters including bond angles and bond lengths are close to reported values.

2.2. Impact of pH

New Journal of Chemistry Accepted Manuscript

 This journal is © The Royal Society of Chemistry 20xx

Please do not adjust margins

View Article Online
DOI: 10.1039/D0NJ03024D

Presence of pH susceptible donor sites in L demands to investigate the influence of pH on spectroscopic properties[53]. It is observed that the emission profile of L remains almost unaltered in the pH span, 3.0 -12.0. Several sets of mixtures of L and pyrene, adjusted to different pH (3.0-12.0) have been tested and found that the difference in emission intensities of L in presence and absence of pyrene is maximum near physiological pH 7.4 (Figure S19, ESI). Hence, the entire experiment has been performed at pH 7.4.

2.3. Effect of medium

Effect of solvent composition on the spectroscopic interaction between L and pyrene have been studied in several semi-aqueous media such as DMSO /H_2O (4/1, v/v); MeOH/H_2O (4/1, v/v); EtOH/H_2O (4/1, v/v); CH_3CN/H_2O (4/1, v/v) and DMF/H_2O (4/1, v/v). Significant interactions, observed in DMSO/H_2O (4/1, v/v) have insisted to monitor the entire studies in this media.[27]

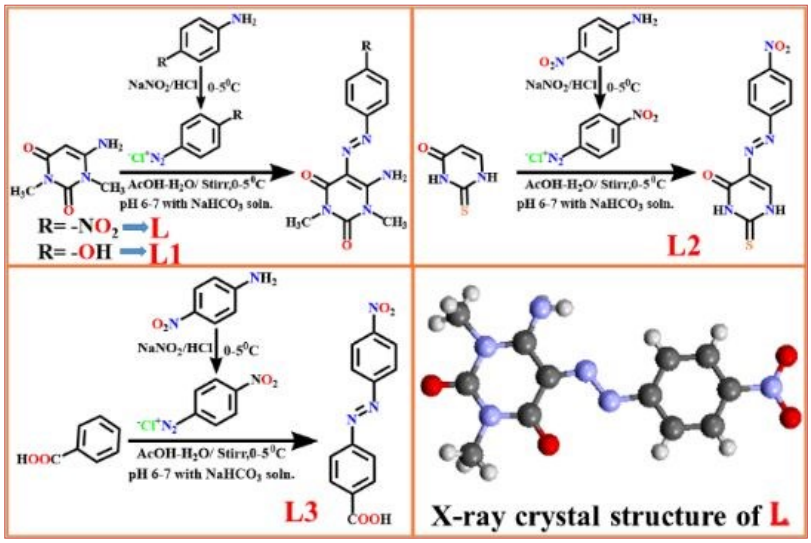

Scheme 1 Synthetic protocol of the probes

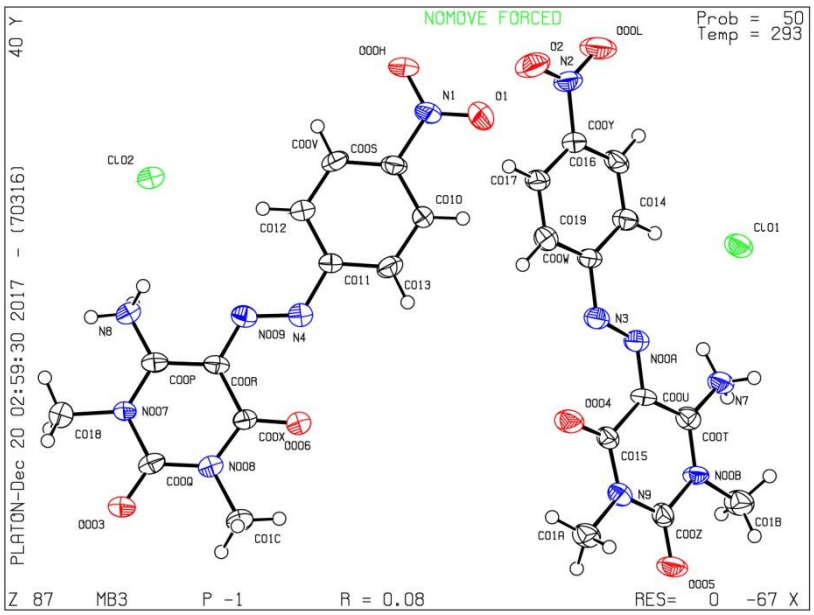

Figure 1 ORTEP view of the L (protonated form)

Published on 12 August 2020. Downloaded by Cornell University Library on 8/15/2020 11:04:24 AM.

New Journal of Chemistry Accepted Manuscript

Please do not adjust margins

View Article Online
DOI: 10.1039/D0NJ03024D

Published on 12 August 2020. Downloaded by Cornell University Library on 8/15/2020 11:04:24 AM.

2.4. Interference studies

The emission spectrum of L is significantly perturbed by pyrene (λ_{Em}, 506 nm, λ_{Ex}, 336 nm) while other tested PAHs like naphthalene (λ_{Em}, 331 nm), anthracene (λ_{Em}, 408 nm), anthanthrene (λ_{Em}, 418 nm), acenaphthene (λ_{Em}, 332 nm), acephenanthrene (λ_{Em}, 298 nm), phenanthrene (λ_{Em}, 292 nm), chrysene (λ_{Em}, 302 nm), benzo[a]pyrene (λ_{Em}, 412 nm), acridine (λ_{Em}, 438 nm), and picene (λ_{Em}, 286 nm) remain silent[38] under similar condition mentioned *supra* (Figure 2).

The same results have been found when the above sets of experiment is monitored by absorption spectroscopy. In presence of pyrene, the absorbance of L significantly enhances at 403 nm while other tested common PAHs remain spectator (Figure 3).

2.5. Spectroscopic monitoring of L-pyrene interaction

Pyrene induces green emission to L without any interference from other tested common PAHs mentioned *supra* (Figure S20, ESI). The changes of emission intensity of L upon gradual addition of pyrene is presented in Figure 4. Upon gradual addition of pyrene to L, the emission intensity at 385 nm decreases while it increases at 506 nm with an iso-emissive point at 445 nm. The formation of a charge transfer (CT) adduct between pyrene (donor) and L (acceptor) through π-π stacking is proposed that inhibits the PET process resulting enhancement of emission intensity by 99-fold and fluorescence quantum yield by 26-fold (λ_{Ex}, 336 nm).

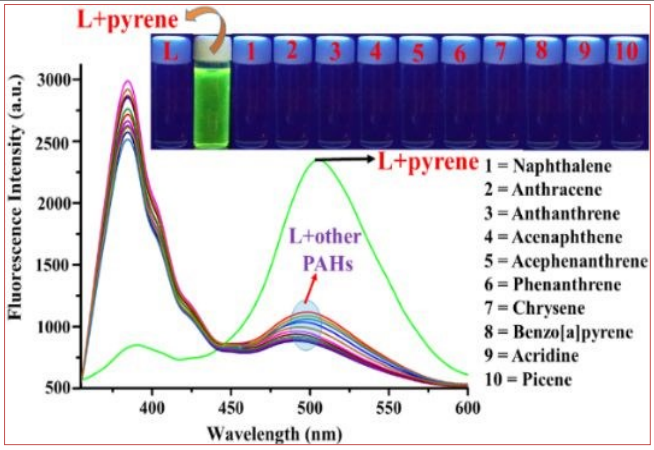

Figure 2

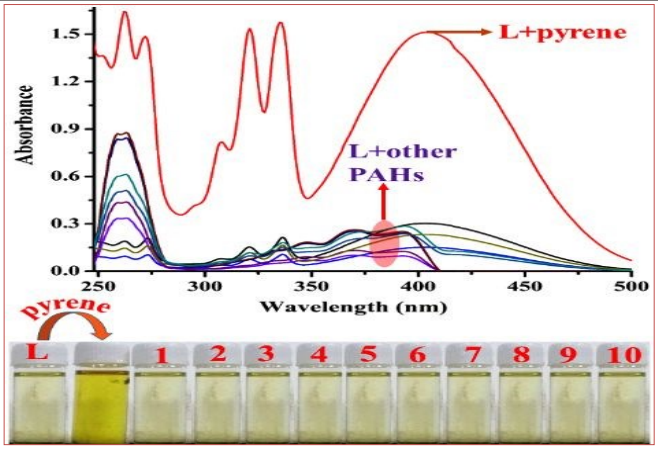

Figure 3

Change in spectra of L (20 μM) in presence of common PAHs: **Figure 2** (Emission, λ_{Ex}, 336 nm) and **Figure 3** (absorption). Media: DMSO/H_2O, 4/1, v/v, 20 mM HEPES buffer, pH 7.4

New Journal of Chemistry Accepted Manuscript

This journal is © The Royal Society of Chemistry 20xx

Please do not adjust margins

View Article Online
DOI: 10.1039/D0NJ03024D

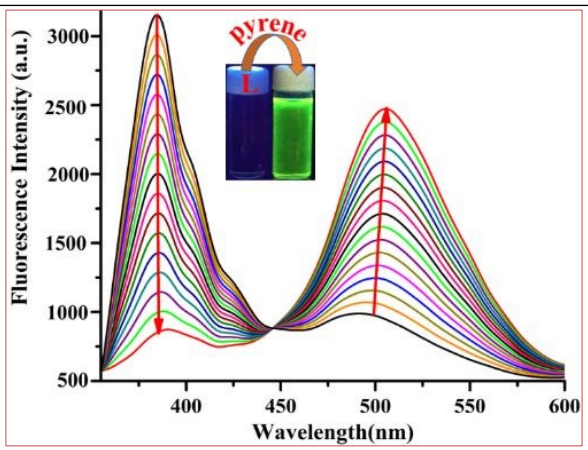

Figure 4 Changes in the emission spectra of L (20 μM) upon addition of pyrene at room temperature in mentioned media (λ_{Ex} = 336 nm); [pyrene] = 0.0001, 0.001, 0.01, 0.1, 1, 10, 100, 400, 600, 800, 1000, 1200, 1400, 1500, 2000, 2500 and 3000 μM).

Likewise, upon gradual addition of pyrene to L, the weak absorption at 403 nm increases while the bare eye pale yellow color turns to intense yellow (Figure 5). Other tested common PAHs (mentioned *supra*) remain spectator without any change in spectra/ color.

The plot of emission intensity *vs.* concentration of pyrene (λ_{Em} = 506 nm, Figure S22, ESI) allows to determine its detection limit, 3.6×10^{-9} M following 3σ/ K method (inset, Figure S21, ESI)[54]. The corresponding interaction constant, determined applying Hill equation[55-56] on fluorescence titration data is 9.59×10^{5} M^{-1} (Figure S22, ESI). The Job's plot[56-57] indicates 1:1 (mole ratio) interaction between L and pyrene (Figure S23a, ESI).

2.6. Sensing mechanism

The L displays weak emission at 373 nm (λ_{Ex} = 336 nm) due to PET process (Figure S5, ESI). Upon addition of pyrene, the emission intensity at 373 nm gradually decreases with concomitant increase at 506 nm (Figure 4). This is primarily due to formation of charge transfer (CT) adduct between pyrene (donor) and azouracil (acceptor) (Scheme S2, ESI). Moreover, [pyrene-L] adduct may exists in static-dynamic excimer equilibrium[37] involving *syn*- and *anti*- forms (Schemes 2-3). To strengthen the proposed CT process, pyrene-1-carboxaldehyde is used instead of pyrene whereby emission intensity remains almost unaltered (Figure S23b, ESI), corroborating our proposition. The presence of electron withdrawing -CHO group (-I effect) hinders the CT process from pyrene moiety to L.

In addition, the [L-pyrene] CT adduct undergoes aggregation in presence of water through inter-molecular hydrogen bond involving $-NH_2$ moiety of L and H_2O that stabilizes the *syn*-form leading to stable static excimer (Scheme 3; Scheme S1, ESI). Thus, water assisted aggregation of [L-pyrene] CT adduct is responsible for significant fluorescence enhancement.

The necessity of water for aggregation of [L-pyrene] CT adduct is reflected in Figure S24 (ESI) where pyrene is gradually added to L in pure DMSO medium, resulting much lower fluorescence enhancement than that observed in aqueous DMSO media.

Published on 12 August 2020. Downloaded by Cornell University Library on 8/15/2020 11:04:24 AM.

New Journal of Chemistry Accepted Manuscript

Please do not adjust margins

View Article Online
DOI: 10.1039/D0NJ03024D

Published on 12 August 2020. Downloaded by Cornell University Library on 8/15/2020 11:04:24 AM.

To further corroborate the proposed sensing mechanism, three model probes, *viz.* L1, L2 and L3 have been designed judiciously (Scheme 1). Interestingly, the L1 contains –OH (+R effect) instead of $–NO_2$ group (-R effect) present in L. Again, L2 has thio-uracil in place of uracil moiety that lacks -CH_3 having +I effect. On the other hand, the L3 is a non-uracil azo-compound. Interestingly, the electron density on the molecule plays a key role to the AIE based recognition involving CT process (Scheme S2). Moreover, the stability and the extent of charge transfer is highly influenced by the electron density on the donor unit. While the presence of $–NO_2$ group lowers the electron density on the aromatic unit and subsequently to the azo-moiety (–N=N–) of L, the reverse is true for L1 due to presence of –OH group. The effect is reflected in the CT process. The experimental results support this line of thinking. Upon gradual addition of pyrene (0.0001-3000 µM) to L (20 µM, DMSO/H_2O, 4/1, v/v), the emission intensity gradually increases from 612 a.u. to 2498 a.u whereas it enhances from 116 a.u. to 456 a.u. for L1 (Figure S25, ESI). The maximum fluorescence enhancement is observed for L2 (128 a.u. - 642 a.u.) indicating strong CT adduct formation with pyrene (Figure S26, ESI). However, lack of $–NH_2$ group at uracil moiety hinders stabilization of its static excimer in presence of water through inter-molecular H-bonding (Scheme S3, ESI). Hence AIE is not observed for L2. Thus, presence of $–NH_2$ group is probably essential for AIE process. On the other hand, failure of L3 to pyrene recognition indicates the necessity of the uracil moiety (Figure S27, ESI).

In addition, general red shift of the FTIR spectrum of the [L-pyrene] adduct compared to free L corroborates their interaction (Figures S4, S28, ESI)[56].

2.7. Dynamic light scattering (DLS) studies

The DLS studies support water assisted aggregation of L in presence of pyrene. Upon gradual addition of pyrene (0.0001 µM to 3000 µM) to L (20 µM), the average particle size (Z_{av}) remain almost unaltered. With increasing water (DMSO to DMSO/H_2O, 4/1, v/v, pH 7.4), the Z_{av} increase to 175 nm, indicating aggregation. The Z_{av} value further enhances from 175 nm to 796 nm with increasing water content from DMSO/H_2O (4/1, v/v) to (1/1, v/v), keeping concentration of L and pyrene unaltered[37] (Figure 6). The DLS study indicates that L1 and L2 remain reluctant towards water assisted AIE based detection of pyrene (Figures S29- S30, ESI).

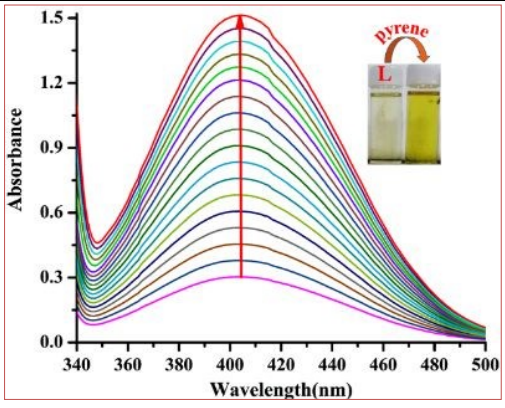

Figure 5 Changes in absorption spectra of L (20 µM) *vs.* [pyrene] in same media; [pyrene] = 0.0001, 0.001, 0.01, 0.1, 1, 10, 100, 400, 600, 800, 1000, 1200, 1400, 1500, 2000, 2500 and 3000 µM).

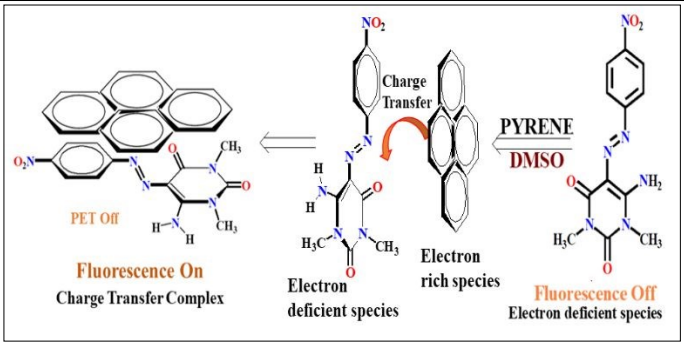

Scheme 2 Charge transfer (CT) adduct

This journal is © The Royal Society of Chemistry 20xx

New Journal of Chemistry Accepted Manuscript

View Article Online
DOI: 10.1039/D0NJ03024D

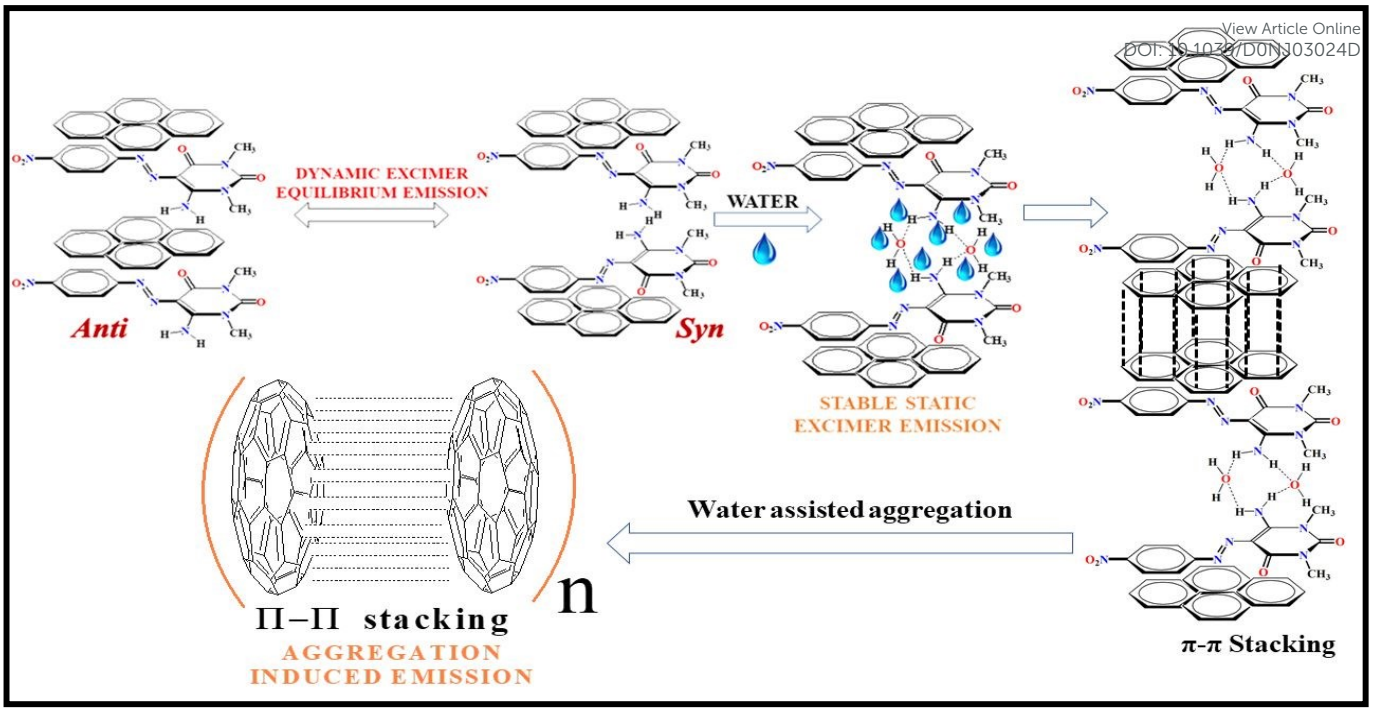

Scheme 3 Plausible sensing mechanism

2.8. ^{1}HNMR titration

The proposed sensing mechanism is further corroborated by ^{1}HNMR titration in DMSO-d_6 (Figure 7). Upon addition of 0.5 equiv. pyrene to L, alkyl protons shifted up-field from 2.46 to 2.39 ppm, indicating their interaction with pyrene. Moreover, 'd' and 'e' protons (Figure S2, ESI) shifted up-field from 7.91 to 7.85 ppm and 8.32 to 8.29 ppm, indicating their interaction with pyrene. On the other hand, 'p' and 'q' protons also shifted up-field from 11.91 and 12.96 ppm respectively. Upon addition of 1.0 equiv. pyrene to L, both 'p' and 'q' protons disappeared indicating plausible tautomerism (between $-NH_2$ and –N=N- functionalities) of L that arose due to π-π interaction with pyrene (Figure S2, ESI). Additionally, all aromatic protons up-field shifted due to enhanced electron density in the ring *via* π-π interaction with pyrene, leading to excimer formation. Upon

addition of 3.0 equiv. pyrene, the peaks broaden, probably due to exchange between free and aggregated forms of L (Figure 7).

Published on 12 August 2020. Downloaded by Cornell University Library on 8/15/2020 11:04:24 AM.

New Journal of Chemistry Accepted Manuscript

View Article Online
DOI: 10.1039/D0NJ03024D

Journal Name

ARTICLE

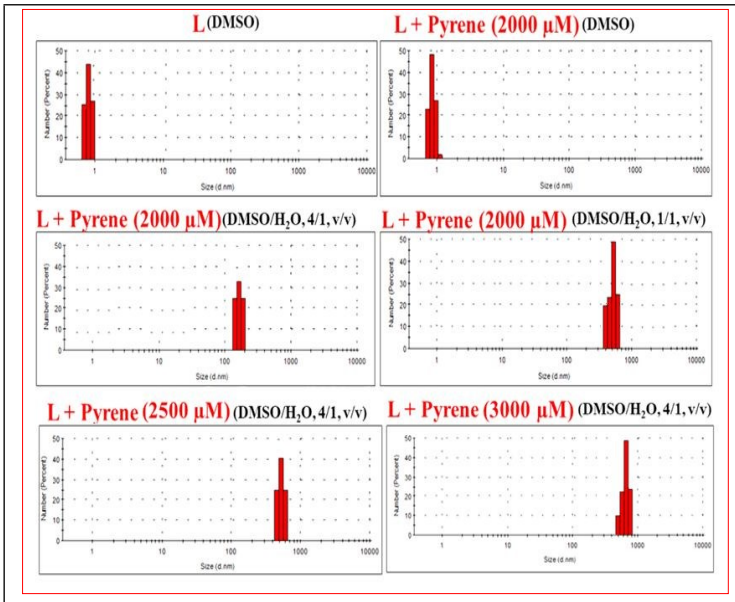

Figure 6 DLS of [L- pyrene] adduct with increasing water content/pyrene content of the media (DMSO/H_2O)

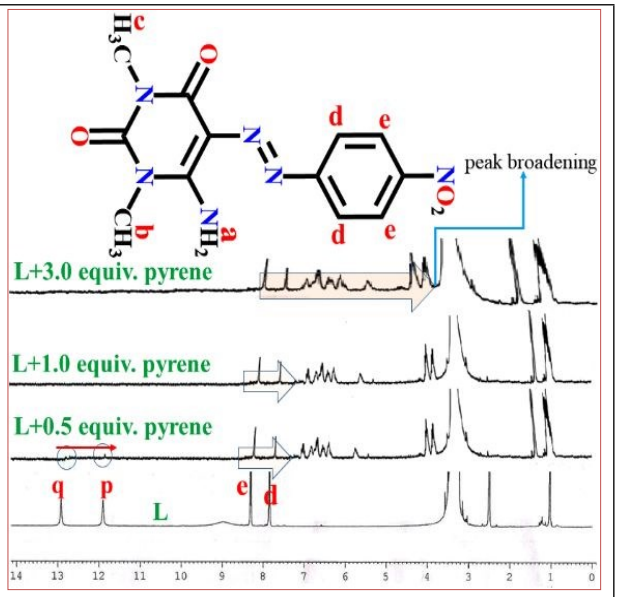

Figure 7 Changes in ^{1}HNMR spectra of L in absence and presence of pyrene in DMSO-d_6 (for signals "p" and "q" see Figure S2.

2.9. Role of water in AIE process

The emission properties of [L-pyrene] adduct is influenced by the water content of the media (DMSO/H_2O) (Figure 8). The emission intensity of L (λ_{Em}, 336 nm) enhances almost 40 fold and 56 fold at 50% H_2O (v/v) and 90% H_2O (v/v) respectively, a signature of aggregation. Further increase of water content results turbidity, hindering measurement of emission intensity.[37] The aggregation process has also been monitored using absorption spectroscopy. Gradual addition of H_2O (25-80%, v/v) to DMSO solution of [L-pyrene] adduct results broadening and red shift of the peak from 403 nm to 437 nm (Figure 9). Side by side presentation of water assisted aggregation of [L-pyrene] adduct (DMSO/ H_2O, v/v), and monomer-excimer emission of pyrene is shown in Figure 10. The ratio of emission intensities (EI) of respective excimers, *viz.* EI $_{[L\text{-pyrene}]}$ at 506 nm/ EI $_{[pyrene]}$ at 461 nm is 16.1 (DMSO/ H_2O, 4/1, v/v, pH 7.4).

2.10. Fluorescence life time studies

The fluorescence life time data corroborate the proposed interaction mechanism (Figure 11). The average life-time of L is 0.236 ns in DMSO. In presence of pyrene (1: 1, mole ratio), the life time increases to 2.2361 ns. Increasing water content gradually enhances the fluorescence life time from 92.2356 ns (25%, v/v). Moreover, the quantum yield [55-58] (ϕ) increases from 5.36% to 26.27%.

Published on 12 August 2020. Downloaded by Cornell University Library on 8/15/2020 11:04:24 AM.

New Journal of Chemistry Accepted Manuscript

Please do not adjust margins

View Article Online
DOI: 10.1039/D0NJ03024D

Published on 12 August 2020. Downloaded by Cornell University Library on 8/15/2020 11:04:24 AM.

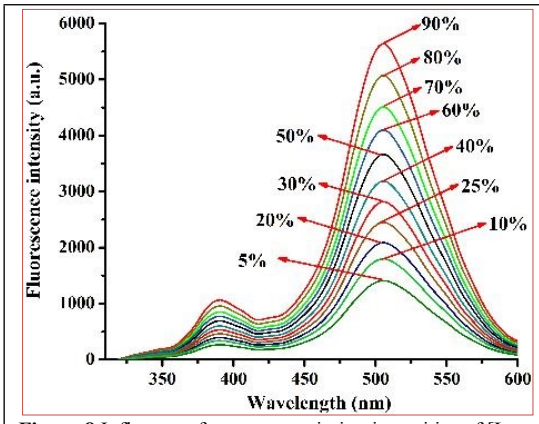

Figure 8 Influence of water on emission intensities of [L-pyrene] adduct (λ_{Ex}, 336 nm) (% indicates water content of the media, DMSO/ H_2O, v/v).

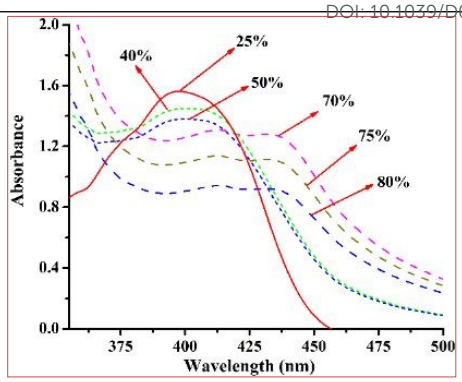

Figure 9 Influence of water on the absorption spectra of [L-pyrene] adduct.

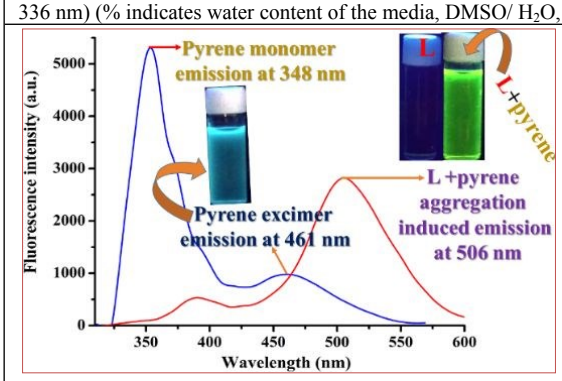

Figure 10 Water assisted aggregation of [L-pyrene] adduct (DMSO/ H_2O, 4/1, v/v, pH 7.4).

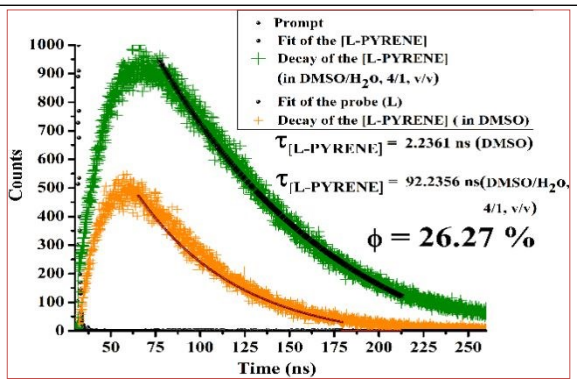

Figure 11 Fluorescence life time decay of [L-pyrene] adduct in presence and absence of water (λ_{Em} = 506 nm).

2.11. Theoretical studies

The geometry of L and [L-pyrene] CT adduct in gas phase have been optimized without restrictions of symmetry in singlet ground state, along with gradient-corrected density functional theory (DFT) with three-parameter fit of exchange and correlation functional of Becke (B3LYP) that include correlation functional of Lee et al. (LYP).[59-61] The method is known as RTD-B3YLP-FC. Their structural parameters are summarized in Tables S3-S4 (ESI). The total energy and dipole moment of the L are -1093.22688 a. u. and 14.1660 Debye respectively. It has C1 point group with a triclinic lattice system. The unit cell lengths are 15.27 (a), 7.50 (b) and 3.46 and c respectively (Figure 12).

Table S4 (ESI) reveals close proximity of experimental and theoretical (non-scale) IR frequencies, in terms of band positions, intensities and shape. The deviations that have been observed are not unusual because theoretical calculations have been performed in gas phase.

The peak at 402 nm in theoretical gas phase absorption spectrum (Figure S30, ESI) matches to that observed experimentally at 403 nm in DMSO/H_2O (4/1, v/v, HEPES buffer, pH 7.4). Theoretical spin-allowed electronic transitions of L are summarized in Table S6 (ESI). Out of 158 orbitals (both alpha and beta), the 79th orbital is HOMO (-0.21524eV) and 80th orbital is LUMO (-0.15295 eV). The HOMO -LUMO energy gap is 0.0623 eV (Figure 13). In [L-pyrene], out of 264

New Journal of Chemistry Accepted Manuscript

Please do not adjust margins

View Article Online
DOI: 10.1039/D0NJ03024D

orbitals (both alpha and beta), the 132th orbital is HOMO (-0.12290eV) and 133th orbital is LUMO (-0.09440 eV). The HOMO -LUMO energy gap is 0.0285 eV (Figure 13). Lower energy gap in [L-pyrene] indicates its stability (Scheme 2). Theoretical spin-allowed electronic transitions of [L-pyrene] are summarized in Table S7 (ESI). TD-DFT calculations (Tables S6-S7) also support experimental findings. The excitation spectrum of the L at 336 nm (Figure S5, ESI) matches the theoretical TD-DFT data at 336 nm and 365 nm of [L-Pyrene] adduct (Table S6- S7).

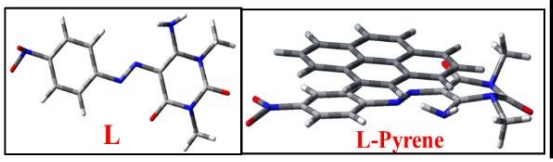

Figure 12 DFT optimized geometry

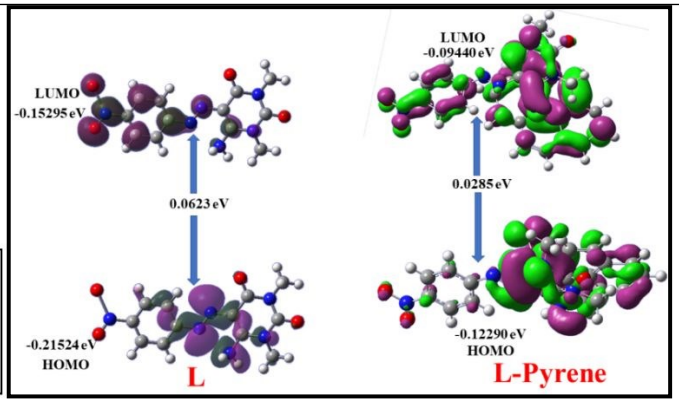

Figure 13 HOMO-LUMO energy gap

2.12. Application

2.12.i. Real sample analysis and solid phase extraction (Table 1)

The L is employed [37-38] to determine pyrene in pond and tap water samples following standard addition method. For this purpose, a known amount of pyrene is added to water samples (collected from pond in Durgapur-Asansol industrial area, one of the most polluted places in West Bengal, India and tap water collected from our research laboratory). The samples are then analysed for determination of pyrene following the developed method (Figure 14).[62]

The immobilization of L on silica (150-200 mesh) have been performed following literature.[62] L (1.5g) and silica (10.5g) are mixed together in 25 mL MeOH and refluxed for 3h while the solution color turns pale yellow (Figure 15). The solvent is removed under vacuum. A glass column (10 cm × 1 cm) is packed with the immobilized L maintaining the bed volume, 10 mL. To establish the binding of silica immobilized L to pyrene, its FTIR spectra is measured before and after sorption of pyrene. Moreover, the L immobilised silica is used for solid phase extraction (SPE) of pyrene[56-58, 62-67] from its reservoir (**Table 2**). The sorbed pyrene on silica immobilised L is eluted by DMSO/H_2O (4/1, v/v) and concentration of pyrene in the eluent is measured by the developed method. Both complete sorption and desorption of pyrene on silica immobilised L is ascertained from non-fluorescence nature of the effluent and eluent, upon exposure of UV-light (Figure 16). Figure S31 (ESI) displays the red shifted FTIR spectrum of the silica immobilized L before and after consuming pyrene. Interestingly, after passing pyrene through silica immobilized L, the bed becomes intense yellow, indicating retention of pyrene by silica immobilized L (Figure 15).

Published on 12 August 2020. Downloaded by Cornell University Library on 8/15/2020 11:04:24 AM.

New Journal of Chemistry Accepted Manuscript

This journal is © The Royal Society of Chemistry 20xx

Please do not adjust margins

View Article Online
DOI: 10.1039/D0NJ03024D

Journal Name

ARTICLE

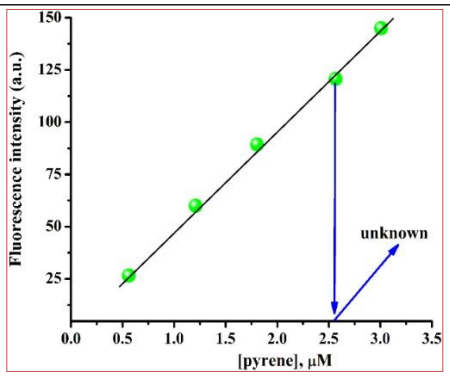

Figure 14 Calibration plot for pyrene estimation.

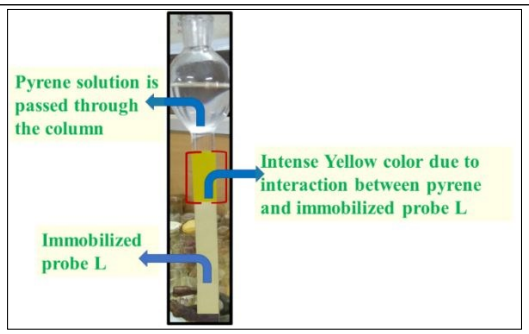

Figure 15 Color of silica immobilized L before and after sorption of pyrene

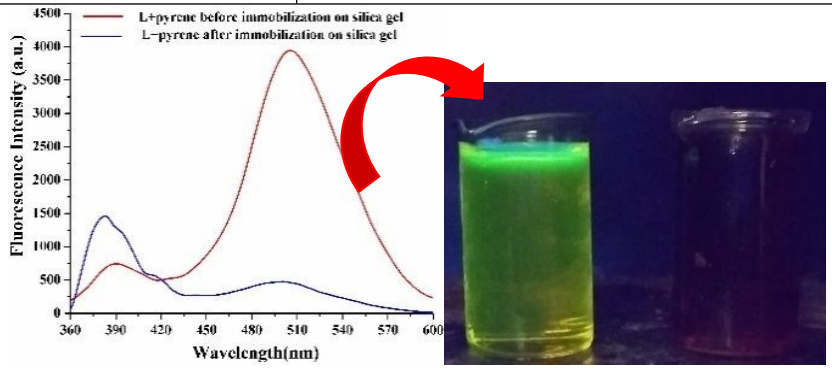

Figure 16 The emission spectra (left) and UV light irradiated colours (right) of the sample before and after passing through silica immobilised L

Table 1 Determination of pyrene in water

Pond water			
Sample No.	**Added (10^{-3} M)**	**Found (10^{-3} M)**	**Recovery (%)**
P1	**20**	**19.56**	**97.80 ± 1.23**
P2	**15**	**14.78**	**98.53 ± 1.03**
P3	**12**	**11.80**	**98.30 ± 1.62**
Tap water			
Sample No.	**Added (10^{-3} M)**	**Found (10^{-3} M)**	**Recovery (%)**
T1	**20**	**19.12**	**95.60 ± 1.26**
T2	**15**	**14.07**	**93.80 ± 1.61**
T3	**12**	**11.16**	**93.01 ± 1.10**

Published on 12 August 2020. Downloaded by Cornell University Library on 8/15/2020 11:04:24 AM.

New Journal of Chemistry Accepted Manuscript

Please do not adjust margins

View Article Online
DOI: 10.1039/D0NJ03024D

Table 2 Solid phase extraction (SPE) of pyrene using silica immobilized L

Solid phase extraction			
Sample	**Pyrene added (10^{-3} M)**	**Pyrene estimated (10^{-3} M)**	**Recovery (%)**
S1	**30**	**28.46**	**94.86±1.12**
S2	**25**	**23.12**	**92.48±1.32**
S3	**20**	**18.78**	**93.90±1.22**

3. Experimental

Materials and equipment used, general method of UV-Vis and fluorescence titration have been discussed in detail in ESI.

3.1. Selectivity and interference studies

Studies on plausible interference from common competing PAHs during pyrene sensing have been performed in two different ways. In first experiment, different competing PAHs are added to the [L-pyrene] system in different sets while in the other, mixture of PAHs including pyrene is added to the L. In first case, the emission intensity remains unaltered while emission intensity increased to the same extent to that of the [L-pyrene] system in second case. These results indicate the selectivity of L for pyrene and non-interference of other competing PAHs during recognition of pyrene by L (Figure S20, ESI).

Thus, to check plausible interference, relative emission intensities of [L-pyrene] (1:1, 20 μM) adduct are measured in presence of other PAH (20 μM) in DMSO/H_2O (4/1, v/v, pH 7.4) (λ_{Ex} = 336 nm).

To check the selectivity of L for pyrene, different PAH (10 mM) is mixed with L (20 μM) in different sets along with a set where all PAHs are mixed together with L. Then the emission intensity of all the sets are measured.

3.2. Effect of pH

The solution of L (100 μM, DMSO/ H_2O, 4/1, v/v) is diluted with HEPES buffer (20 mM) solution to prepare working solution of L (20 μM) of appropriate pH (3.0 to 12.0). Then, pyrene (37.5 mg, 0.18 mmol, 20 μM) dissolved in HEPES buffer is added to the solution of L (20 μM) in different sets, maintained at different pH. The emission intensities of different sets of solutions are measured at room temperature.

3.3. ^{1}H NMR titration

Three different sets containing L (3.56 mg dissolved in 700 μL DMSO-*d*6) and pyrene (0.5, 1.0, 3.0 equiv. pyrene dissolved in minimum volume of D_2O) are prepared by sonication and ^{1}HNMR spectra of the mixture are recorded.

3.4. Calculation of detection limit

For this purpose, fluorescence titration of L with pyrene is performed. The concentration at which a sharp change in emission intensity is observed, multiplied by the concentration of L to calculate the detection limit.[62]

3.5. Determination of association constant

The binding constant calculated using Hill's equation,[62] $\log[Y/(1-Y)] = n \log[G] + \log Kapp$ where, Y, n, [G] and $Kapp$ represent the fraction of L binding sites filled, Hill coefficient, concentration of pyrene and association constant respectively.

Published on 12 August 2020. Downloaded by Cornell University Library on 8/15/2020 11:04:24 AM.

New Journal of Chemistry Accepted Manuscript

This journal is © The Royal Society of Chemistry 20xx

Please do not adjust margins

View Article Online
DOI: 10.1039/D0NJ03024D

Published on 12 August 2020. Downloaded by Cornell University Library on 8/15/2020 11:04:24 AM.

The value of Hill coefficient describes the cooperativity of L binding in the following way: n > 1, positive cooperativity; n = 1, non-cooperativity and n < 1, negative cooperativity. *Y* is determined by the equation of $(F_x\text{-}F_0)/(F_{max}\text{-}F_x)$, where F_0, F_x, and F_{max} are the emission intensities of L in absence of pyrene, at an intermediate pyrene concentration, and at a concentration of complete interaction respectively. The value of *K* thus evaluated is 9.59×10^5 M^{-1}, indicating strong interaction between the L and pyrene.

3.6. Determination of quantum yield

The fluorescence quantum yields of L and its adduct with pyrene are determined using pyrene as reference with a known ϕ_R value, 0.2 in DMSO/H_2O (4/1, v/v, HEPES buffer, pH 7.4).[64] The L, **[**L-pyrene] adduct and reference dye are excited at 336 nm, maintaining almost equal absorbance (0.1) and emission intensities. The area of the emission spectrum is integrated using the software available in the instrument and the quantum yield is calculated following the equation [64], $\phi_S/\phi_R = [A_S/A_R]\times[(Abs)_R/(Abs)_S]\times[\eta_S^2/\eta_R^2]$ where ϕ_S and ϕ_R are the fluorescence quantum yield of the sample and reference respectively, A_S and A_R are area under the emission spectra of the sample and reference respectively, $(Abs)_S$ and $(Abs)_R$ are optical densities of the sample and reference solution at corresponding excitation wavelength; η_S and η_R are refractive indices of the sample and reference respectively.[68-69]

3.7. Synthesis

3.7.1. General method (Scheme 1)

The azo compounds[37] that have been synthesized are 6-amino-1,3-dimethyl-5-(4-nitro-phenylazo)-1H-pyrimidine-2,4-dione (L), 6-amino-5-(4-hydroxy-phenylazo)-1,3-dimethyl-1H-pyrimidine-2,4-dione (L1), 5-(4-nitro-phenylazo)-2-thioxo-2,3-dihydro-1H-pyrimidin-4-one (L2) and 4-(4-nitro-phenylazo)-benzoic acid (L3). In general, diazotization of acidic solution of respective amine (1.0 mmoL, 138 mg for L, L2 and L3 while 139 mg for L1) using sodium nitrite (76 mg, 1.1 mmol) at 0-5^{0}C followed by coupling with 6-amino-1, 3-dimethyl uracil (1.0 mmoL, 155 mg for L and L1, 128 mg 2-thiouracil for L2 and 122 mg benzoic acid for L3), dissolved in saturated sodium bicarbonate solution at pH 6-7. The colourful solid azo compounds are separated by filtration and dried in *vacuuo*.

L

The yellow L is obtained in 97% yield. Anal. calcd. for $C_{12}H_{12}N_6O_4$ (%): C, 43.37; H, 3.98 and N, 27.62; found, C, 43.87; H, 4.01 and N, 27.97. QTOF–MS ES(+) (Figure S1, ESI) $[M + H]^+$ = 305.1259 (100%), $[M+Na]^+$ = 327.1095 (17%). ^{1}HNMR (Figure S2, ESI) (DMSO-d_6, δ, ppm): 12.92 (s, 1H, =NH), 11.91 (s, 1H, =N-NH, azo moiety); 8.32-8.30 (d, 2H, Ar–H); 7.86-7.85 (d, 2H, Ar–H); 3.37-3.26 (m, 6H, N–CH_3); 3.24 (s, 2H, -NH_2); ^{13}CNMR (Figure S3, ESI) (DMSO-d_6, δ, ppm): 28.46 (-CH_3); 28.57 (-CH_3); 29.27 (-CH_3); 30.07 (-CH_3); 121.76 (=CH); 125.64 (=CH); 146.02 (-C=O); 146.77 (-C=O); 150.04 (=C-NH_2). FTIR (cm^{-1}) (Figure S4, ESI) υ(–NH_2), 3546; ν(aromatic C–H), 2976; υ(sp^{3}C-H), 1651; υ(–C=C), 1500; υ(–N=N–), 1448; υ(–C–N), 1303. The L emits at 373 nm (λ_{Ex} = 336 nm, Figure S5, ESI). The absorption spectrum of L (20 μM, DMSO/H_2O, 4/1, v/v, HEPES buffer, pH 7.4) exhibits strong peaks at 256 nm ($\varepsilon = 8.8\times10^5\ M^{-1}\ cm^{-1}$) and 403 nm ($\varepsilon = 5.66\times10^3\ M^{-1}\ cm^{-1}$) (Figure S5, ESI).

New Journal of Chemistry Accepted Manuscript

Please do not adjust margins

View Article Online
DOI: 10.1039/D0NJ03024D

Published on 12 August 2020. Downloaded by Cornell University Library on 8/15/2020 11:04:24 AM.

L1

The red-brown compound is obtained in 94% yield. Anal. calcd. for $C_{12}H_{13}N_5O_3$ (%): C, 52.36; H, 4.76; N, 25.44; found, C, 52.37; H, 4.71 and N, 25.47. QTOF–MS ES(+) (Figure S6, ESI) $[L1+Na]^+$ = 298.4137 (100%), $[L1+CH_3OH+H]^+$ =308.3629 (17%); ^{1}HNMR (Figure S7, ESI) (DMSO-d_6, δ, ppm): 13.48 (s, 1H, –N-NH); 12.49 (s, O-H); 8.71-8.69 (d, 2H, Ar–H); 7.54-7.44 (d, 2H, Ar–H); 3.07-3.04 (m, 6H, N–CH_3); 3.02 (s, 2H, -NH_2); FTIR (cm^{-1}) (Figure S8, ESI) υ(–NH_2), 3321; ν(–O–H), 3144; υ(–C=O), 1718,1669; υ(–C=C), 1516; υ(–N=N–), 1441; υ(–C–N), 1293. The L1 emits at 396 nm (λ_{Ex} = 302 nm, Figure S9, ESI).

L2

The yellow compound is obtained in 82% yield. Anal. calcd. for $C_{10}H_7N_5O_3S$ (%): C, 43.32; H, 2.54; N, 25.26; found, C, 43.34; H, 2.51 and N, 25.27. QTOF–MS ES(+) (Figure S10, ESI) $[L2+H]^+$ = 278.4180 (93%), $[L2+CH_3OH+H]^+$ =310.6752 (80%); ^{1}HNMR (Figure S11, ESI) (DMSO-d_6, δ, ppm): 7.93-7.91 (d, 2H, Ar–H); 7.56-7.54 (d, 2H, Ar–H); 7.40 (s, 1H, –C=C–H); 5.82 (s, 1H, S=C-NH–C=O); 5.80 (s, 1H, S=C-NH–HC); FTIR (cm^{-1}) (Figure S12, ESI) υ(–NH_2), 3454; υ(–C=O), 1708,1678; υ(–C=C), 1565; υ(–N=N–),1506; υ(–NO_2), 1376; υ(–C–N), 1216. The L2 emits at 388 nm (λ_{Ex} = 300 nm, Figure S13, ESI).

L3

The brown compound is obtained in 89% yield. Anal. calcd. for $C_{13}H_9N_3O_4$ (%): C, 57.57; H, 3.34; N, 15.49; found, C, 57.54; H, 3.35 and N, 15.47. QTOF–MS ES(+) (Figure S14, ESI) $[L3+H_2O+H]^+$ = 290.3860(98%), $[L3+Na]^+$ = 294.1680 (56%); ^{1}HNMR (Figure S15, ESI) (DMSO-d_6, δ, ppm): 8.46-8.44 (d, 2H, Ar–H); 8.22-8.11 (d, 2H, Ar–H); 7.61–7.58 (d, 2H, Ar–H); 7.48–7.41 (d, 2H, Ar–H); FTIR (cm^{-1}) (Figure S16, ESI) υ(–O–H), 3454; υ(–C=C), 1560; υ(–N=N–),1483; υ(–NO_2), 1388; υ(–C–N), 1340, υ(–C–O), 1109. The L3 emits at 351 nm (λ_{Ex} = 282 nm, Figure S17, ESI).

4. Conclusion

Single crystal X-ray structurally characterized azo-uracil derivative (L) is exploited for selective detection of pyrene at nano-molar in aqueous DMSO media via aggregation induced green emission with 99-fold fluorescence enhancement. The pyrene assisted inhibition of photo-induced electron transfer (PET) in L is triggered by water leading to AIE enhancement through static-dynamic excimer equilibrium involving *syn* and *anti*-forms of L in the charge transfer (CT) complex. Studies on other three model compounds, *viz.* L1, L2 and L3 help to elucidate the interaction process. The interaction constant and LOD values are 9.59×10^5 M^{-1} and 3.6×10^{-9} M respectively. The developed method is useful for trace level determination of pyrene in real samples. Silica immobilised L efficiently removes pyrene from its reservoir. The present report is not only a new method of pyrene detection at nanomolar level, it explores a new horizon in the field of AIE.

Conflicts of interest

No conflicts to declare.

Acknowledgement

MB sincerely acknowledges State DST (West Bengal) for fellowship. MG is grateful to CSIR (New Delhi) for fellowship.

5. Reference

This journal is © The Royal Society of Chemistry 20xx

New Journal of Chemistry Accepted Manuscript

View Article Online
DOI: 10.1039/D0NJ03024D

1. C. T. Chen, *Chem. Mater*. 2004, **16**, 4389–4400.
2. M. E. Germain and M. J. Knapp, *Chem. Soc. Rev*., 2009, **38**, 2543-2555.
3. J. F. Collins, J. P. Brown, S. V. Dawson, and M. A. Marty, *Regul Toxicol Pharmacol.,* 1991, **13**, 170-184.
4. K. Srogi, *Environ Chem Lett*., 2007, **5**, 169–195.
5. D. F. Kalf, T. Crommentuijn, and E. J. V. D. Plassche, *Ecotoxicol Environ Saf.,* 1997, **36**, 89-97.
6. B. J. Finlayson-Pitts, and Jr. J.N. Pitts, *Science*, 1997, **276**, 1045–1052.
7. Z. Fiala, A. Vyskocil, V. Kraják, V. Masín, S. Emminger, V. Srb and J. Tejral, *Acta Medica*, 1999, **42**, 77–89.
8. (a) R. Goldman, L. Enewold, E. Pellizzari, J. B. Beach, E. D. Bowman, S. S. Krishnan and P. G. Shields, *Cancer Res.*, 2001, **61**, 6367–6371. (b) Agency for Toxic Substances and Disease Registry (ATSDR). Toxicological profile for naphthalene. Atlanta, GA: U. S. Department of Health and Human Services; 1996.
9. C. E. Boström, P. Gerde, A. Hanberg, B. Jernström, C. Johansson, T. Kyrklund, A. Rannug, M. Törnqvist, K. Victorin, and R. Westerholm, *Environ Health Perspect.* 2002, **3**, 451-488.
10. H. Choi, and J. Spengler, *Environ Int.*, 2014, **63**, 173-181.
11. M. J. Benecky, C. G. Kolvenbach, R. W. Wine, J. P. DiOrio and M. W. Mosesson, *Biochemistry*, 1990, **29**, 3082−3091.
12. M. J. Benecky, R. W. Wine, C. G. Kolvenbach, and M. W. Mosesson, *Biochemistry*, 1991, **30**, 4298−4306.
13. (a) S. Ouvrard, P. Leglize and J. L. Morel., *Int J Phytoremediation.,* 2014, **16**, 46-61. (b) S. A. Nsibande, and P. B. C. Forbes, *RSC Adv.,* 2020, **10**, 12119-12128.
14. M. Machala, J. Vondracek, L. Blaha, M. Ciganek, and J.V. Neca, *Mutat Res*., 2001, **497**, 49-62.
15. Y. Zhang, S. Dong, H. Wang, S. Tao and R. Kiyama. *Environ Pollut.*, 2016, **213**, 809-824.
16. J. Zhang, L. Chang, H. Jin, Y. Xia, L. Wang, W. He, W. Li, And H. Chen, *Exp Biol Med.*, 2016, **241**, 1516-1523.
17. H. A. Herner, J. E. Trosko and S. J. Masten, *Environ. Sci. Technol*., 2001, **35**, 3576–3583.
18. T. Yoshikawa, L. P. Ruhr, W. Flory, D. Giamalva, D. F. Church and W. Pryor, *Toxicol. Appl. Pharm*., 1985, **79**, 218-226.
19. Z. Zhang, Z. Zhang, H. Lu, Q.Yang, H. Wu, J.Wang, and J. Wu, *Mol Neurobiol*. 2017, **54**, 1874–1886.
20. L. Bielská, M. Kah, G. Sigmund, T. Hofmann, and S. Höss, *Sci. Total Environ.*, 2017, **595**, 132–140.
21. M. Ahmad, A.U. Rajapaksha, J. E. Lim, M. Zhang, N. Bolan, D. Mohan, M. Vithanage, S.S. Lee, and Y.S. Ok, *Chemosphere*, 2014, **99**, 19–33.
22. J. Akkanen, And J.V.K. Kukkonen, *Environ. Toxicol. Chem*., 2003, **22**, 518–524.
23. P. C. Conlon, J. Yang, Y. Wu, Y. Chen, K. Martinez, Y. Kim, N. Stevens, A. A. Marti, S. Jockusch, N. J.

Published on 12 August 2020. Downloaded by Cornell University Library on 8/15/2020 11:04:24 AM.

New Journal of Chemistry Accepted Manuscript

View Article Online
DOI: 10.1039/D0NJ03024D

Turro, and W. Tan, *J. Am. Chem. Soc*., 2008, **130**, 336–342.

24. M. M. McCallister, M. Maguire, A. Ramesh, Q. Aimin, S. Liu, H. Khoshbouei, M. Aschner, F. F. Ebner, and D. B. Hood, *NeuroToxicology*., 2008, **29**, 846–854.
25. R.S. Clark, S.T. Pellom, B. Booker, A. Ramesh, T. Zhang, A. Shanker, M. Maguire, P.D. Juarez, M. J. Patricia, M. A. Langston, M.Y. Lichtveld and D. B. Hood, *Environ Research*. 2016, **146**, 173–84.
26. A. Ramesh, F. Inyang, D.D. Lunstra, M.S. Niaz, P. Kopsombut, K. M. Jones, D.B. Hood, E.R. Hills, and A.E. Archibong, *Exp Toxicol Pathol*., 2008, **60**, 269-80.
27. IARC Monographs, Supplement/World Health Organization, *International Agency for Research on Cancer,* 1987, **7**, 1–440.
28. R. Sinha, M. Kulldorff, M. J. Gunter, P. Strickland and N. Rothman, *Adenoma Cancer Epidemiol Biomarkers Prev.*, 2005, **14**, 2030-2036.
29. M. F. Denissenko, A. Pao, M. Tang and G. P. Pfeifer, *Science*, 1996, **18**, 430-432.
30. J. Gündel, and J. Angerer, *J Chromatogr Sep Tech*, 2000, **738**, 47-55.
31. R. P. Haugland, M. T. Z. Spence, I. D. Johnson, and A. Basey, *The handbook: A guide to fluorescent probes and labeling technologies*, *10th ed., Molecular Probes, Eugene,* 1995.
32. D. S. Karpovich, and G. J. Blanchard, *J. Phys. Chem*., 1995, **99**, 3951−3958.
33. T. Annable, R. Buscall, R. Ettelaie, and D. Whittlestone, *J. Rheol*. 1993, **37**, 695−726.
34. C. Krejtschi and K. Hauser, *Eur. Biophys. J.* 2011, **40**, 673−685.
35. T. A. Pham, F. Song, M.-T. Nguyen and M. Stöhr, *Chem. Commun*., 2014, **50**, 14089-14092.
36. S. Samanta, S. Goswami, Md. N. Hoque, A. Ramesh and G. Das, *Chem. Commun*., 2014, **50**, 11833-11836.
37. (a) A. Ghosh, A. Sengupta, A. Chattopadhyay and D. Das, *Chem. Commun*., 2015, **51**, 11455-11458; (b) V. N. S. Occello, A. V. Veglia, *Anal. Chim. Acta*., 2011**, 689***,* 97-102.
38. (a) S. Nandi, S. Adhikari, S. Mandal, A. Banerjee and D. Das, *J Mol Recognit*., 2016, **29**, 303-307. (b) A. Malik, P. Verma, A. K. Singh and K. P. Singh, *Environ. Monit. Assess.* 2011, **172**, 529–545.
39. R. Gautam, A. Srivastava, and S. M. Jachak, *Phytochem. Anal.,* 2011, **22**, 153-157.
40. A.; Chattererjee, M.; Santra, N.; Won, S. Kim, J.K. Kim, S.B. Kim, and K.H. Ahn, *J. Am. Chem. Soc*., 2009, **131**, 2040-2041.
41. M. Ghosh, S. Mandal, S. Ta, and D. Das, *Sens. Actuators B Chem.*, 2017, **249**, 339-347.
42. B.-R. Gao, H.-Y. Wang, Y.-W. Hao, L.-M. Fu, H.-H. Fang, Y. Jiang, L. Wang, Q. D. Chen, H. Xia, L.-Y. Pan, Y.-G. Ma, and H.-B. Sun, *J. Phys. Chem. B.*, 2010, **114**, 128-134.
43. M. Ghosh, S. Ta, S. Lohar, S. Das, P. Brandão, V. Felix and D. Das, *J. Mol. Recognit.*, 2019, **32**, e2771.

Published on 12 August 2020. Downloaded by Cornell University Library on 8/15/2020 11:04:24 AM.

New Journal of Chemistry Accepted Manuscript

This journal is © The Royal Society of Chemistry 20xx

View Article Online
DOI: 10.1039/D0NJ03024D

44. (a) A. Patasz, and D. Ciez, *Eur. J. Med. Chem.,* 2015, **97**, 582-611. (b) N. Boudet, and P. Knochel, *Org. Lett.,* 2006, **8**, 3737-3740.

45. D. Debnath, S. Roy, B.-H. Li, C.-H. Lin and T. K. Misra, *Spectrochim. Acta A*, 2015, **140**, 185–197.

46. R. Karpicz, V. Gulbinas, and A. Undzenas, *J. Chin. Chem. Soc*., 2000, **47**, 589–595.

47. M.A. Metwally, E. A. Latif, F.A. Amer, and G. Kaupp, *Dyes Pigm*., 2004, **60**, 249–264.

48. Y.K. Zhao, W.B. Chang, and Y.X. Ci, *Talanta*, 2003, **59**, 477–484.

49. N. Menek, E. Eren, and S. Topcu, *Dyes Pigm.*, 2006, **68**, 205–210.

50. D. Rawata, S. R. Sharma, S. Karmakara, A. L. Singh and V. Mishra, *Ecotoxicol. Environ.* 2018, **148**, 528-537.

51. (a) E. Merino, *Chem. Soc. Rev*., 2011, **40**, 3835–3853; (b) T. A. Farghaly and Z. A. Abdallah, *Arkivoc*, 2008, **17**, 295-305. (c) J. Sivamani and A. Siva, *Sens. Actuators B Chem,* 2017, **242**, 423-433. (d) M. Banerjee, M. Ghosh, S. Pradhan, J. S. Matalobos, A. Rej, S. K. Hira, and D. Das. *ACS Appl. Bio Mater.,* 2019, **2**, 1184−1196.

52. (a) C. Carrillo-Carrión, B. M. Simonet and M. Valcárcel, *Anal. Chim. Acta*, 2009, **652**, 278–284. (b) Nsibande S. A. and Forbes P. B. C, *RSC Adv*., 2020, **10**, 12119–12128. (c) O. Adegoke and P.B.C. Forbes, *Talanta*, 2015, **146**, 780-788. (d) S.A. Nsibande, H. Montaseri and P.B.C. Forbes, *Trends Anal. Chem*. 2019, **115**, 52-69. (e) L. Wang, Z. Huang, Q. Gao, Y. Liu, X. Kou and D. Xiao, *Spectrosc Lett.*, 2015, **48**, 748-756. (f) R. A. Wilson, C. J. Seliskar, G. Talaska, and W. R. Heineman, *Anal. Chem.*, 2011, **83**, 3725–3729.

53. (a) S. Piotto, S. Concilio, L. Sessa, R. Diana, G. Torrens, C. Juan, U. Caruso, and P. Iannelli, *Molecules*, 2017, **22**, 1372. (b) A. Ghorai, J. Mondal, R. Chandra and G. K. Patra. *Dalton Trans*., 2015, **44**, 13261-13271. (c) M. Ghosh, S. Ta, J. S. Matalobos and D. Das, *Dalton Trans*., 2018, **47**, 11084-11090.

54. M. Ghosh, S.Ta, M. Banerjee, M. Mahiuddin, S. Khanra, S. K. Hira, P. P. Manna, and D. Das, *J. Photochem. Photobiol. A.*, 2018, **367**, 32-38.

55. Y. G. Sidir, İ. Sidir, H. Berber and E. Taşal, *J. Mol. Liq.,* 2011, **162**, 148-154.

56. M. Ghosh, S. Ta, M. Banerjee, Md. Mahiuddin, and D. Das, *ACS Omega*, 2018, **3**, 4262–4275.

57. A. Ghorai, J. Mondal, R. Chandra and G. K. Patra. *Dalton Trans*., 2015, **44**, 13261-13271.

58. (a) M. Ghosh, A. Ghosh, S. Ta, J. S. Matalobos, and D. Das. *ChemistrySelect*, 2017, **2**, 7426–7431. (b) M. Banerjee, S. Ta, Ghosh, M. Ghosh, A. and D. Das, *ACS Omega,* 2019, **4**, 10877-10890.

59. A. Pandey, S. K. Ashthana, A. Prakash, J. K. Roy, I. Tiwari, and K. K. Upadhyay, *Dalton Trans*., 2019, **48**, 2068-2076.

60. A. Bhattacharya, J. P. Naskar, S. Majumder, R. Ganguly, P. Mitra and S. Chowdhury, *Inorg. Chim. Acta,* 2015, **425**, 124-133.

Published on 12 August 2020. Downloaded by Cornell University Library on 8/15/2020 11:04:24 AM.

New Journal of Chemistry Accepted Manuscript

View Article Online
DOI: 10.1039/D0NJ03024D

61. P. Saha, J. Naskar, A. Bhattacharya, R. Ganguly, B. Saha and S. Chowdhury, *J. Coord. Chem*., 2016, **69**, 303-317.

62. (a) C. Lee, W. Yang, R. G. Parr, *Phys. Rev. Sect. B*, 1988, **37**, 785-789; (b) P.J. Hay, W.R. Wadt, *J. Chem. Phys.*, 1985, **82**, 270-295.

63. (a) A. Sahana, S. Das, A. Banerjee, S. Lohar, D. Karak, D. Das, *J Haz. Mater.*, 2011, **185**, 1448–1457. (b) S. Adhikari, A. Ghosh, M. Ghosh, Guria, S. and D. Das, *Sens. Actuators B: Chem*., 2017, **251**, 942-950. (c) M. Banerjee, M. Ghosh, S. Ta, J. Das, and D. Das, *J. Photochem. Photobiol.* A, 2019, **377**, 286–297.

64. (a) M. Ghosh, S. Ta, M. Banerjee, M. Mahiuddin, P.P. Manna, and D. Das, *ChemistrySelect* 2018, **3**, 6145-6151; (b) A. Ghorai, J. Mondal, S. Bhattacharya, and G. K. Patra, *Anal. Methods,* 2015, **7**, 10385-10393.

65. S. Shit, M. Nandy, D. Saha, L. Zhang, W. Schmitt, C. Rizzoli & T.N, Guru Row, *J. Coord. Chem.*, 2016, **69**, 2403-2414.

66. A. Ghosh, S. Ta, M. Ghosh, S. Karmakar, A. Banik, T. K. Dangar, S. K. Mukhopadhyay and D. Das, *Dalton. Trans.*, 2016, **45**, 599-606.

67. Y. Shen, Z. Liu, X. Yang, H. Wang, Z. Chai, and D. Wang, *Ind. Eng. Chem. Res*., 2017, **56**, 12708–12716.

68. (a) B. F. Parker, Z. Zhang, L. Rao and J. Arnol *Dalton Trans*., 2018, **47**, 639-644.

69. W. H. Melhuish, *J. Phys. Chem.*, 1961, **65**, 229-235.

70. F. I. El-Dossoki, *J .Chin. Chem. Soc.*, 2007, **54**, 1129-1137.

Published on 12 August 2020. Downloaded by Cornell University Library on 8/15/2020 11:04:24 AM.

New Journal of Chemistry Accepted Manuscript

This journal is © The Royal Society of Chemistry 20xx

View Article Online
DOI: 10.1039/D0NJ03024D

Published on 12 August 2020. Downloaded by Cornell University Library on 8/15/2020 11:04:24 AM.

Graphical abstract

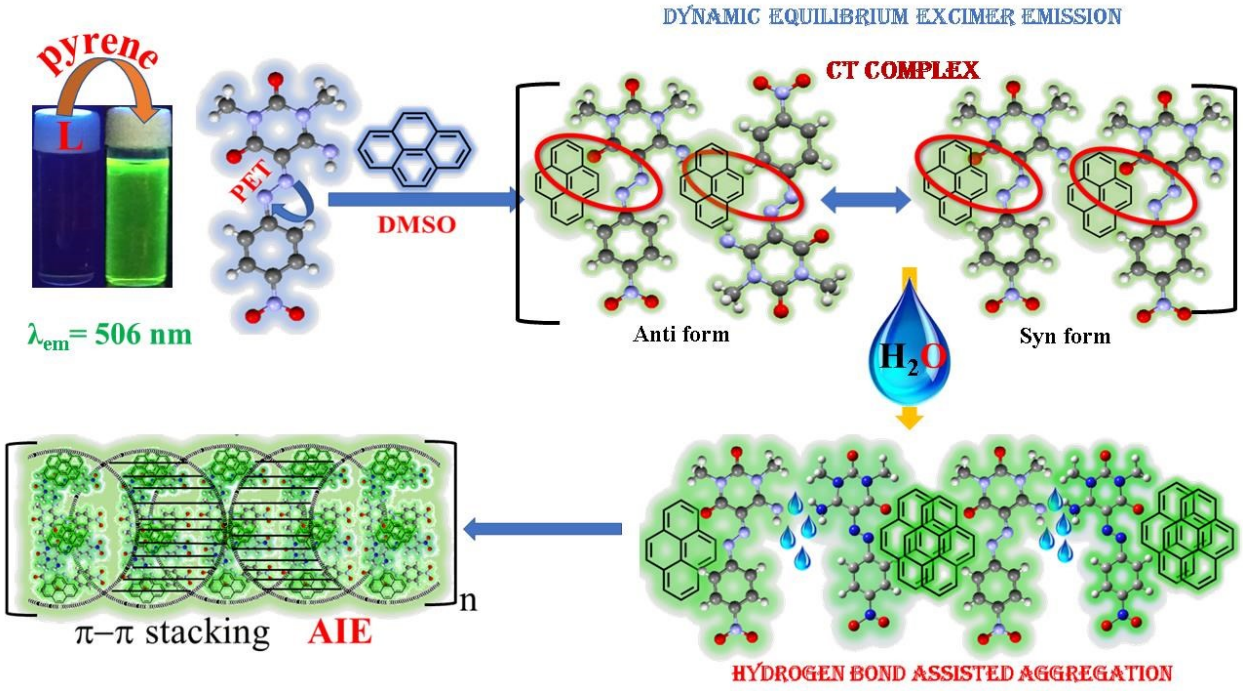

New Journal of Chemistry Accepted Manuscript